General Disclaimer

One or more of the Following Statements may affect this Document

- This document has been reproduced from the best copy furnished by the organizational source. It is being released in the interest of making available as much information as possible.

- This document may contain data, which exceeds the sheet parameters. It was furnished in this condition by the organizational source and is the best copy available.

- This document may contain tone-on-tone or color graphs, charts and/or pictures, which have been reproduced in black and white.

- This document is paginated as submitted by the original source.

- Portions of this document are not fully legible due to the historical nature of some of the material. However, it is the best reproduction available from the original submission.

Produced by the NASA Center for Aerospace Information (CASI)

PHASE 2 OF THE ARRAY AUTOMATED ASSEMBLY TASK

FOR THE LOW COST SOLAR ARRAY PROJECT

R. B. Campbell, P. Rai-Choudhury, E. J. Seman,
A. Rohatgi, J. R. Davis, J. Ostroski and
R. W. Stapleton

Quarterly Report No. 6
January 1, 1979 - March 31, 1979

May 15, 1979

Contract No. 954873

This work was performed for the Jet Propulsion Laboratory, California Institute of Technology, under NASA Contract NAS7-100 for the U. S. Department of Energy, Division of Solar Energy.

The JPL Low Cost Solar Array Project is funded by DOE and forms part of the DOE Photovoltaic Conversion Program to initiate a major effort towards the development of low cost solar arrays.

(NASA-CR-158727) ARRAY AUTOMATED ASSEMBLY TASK FOR THE LOW COST SOLAR ARRAY PROJECT, PHASE 2 Quarterly Report, 1 Jan. - 31 Mar. 1979 (Westinghouse Research and) 50 p HC A03/MF A01 CSCL 10A G3/44

N79-26489

Unclas
27810

JUL 1979
RECEIVED
NASA STI FACILITY
ACCESS DEPT.

Westinghouse R&D Center
1310 Beulah Road
Pittsburgh, Pennsylvania 15235

TECHNICAL CONTENT STATEMENT

This report was prepared as an account of work sponsored by the United States Government. Neither the United States nor the United States Department of Energy, nor any of their employees, nor any of their contractors, sub-contractors, or their employees, makes any warranties, express or implied, or assumes any legal liability or responsibility for the accuracy, completeness or usefulness of any information, apparatus, product or process disclosed, or represents that its use would not infringe privately owned rights.

NEW TECHNOLOGY

No new technology is reportable for the period covered by this report.

TABLE OF CONTENTS

PRECEDING PAGE BLANK NOT FILMED

LIST OF FIGURES

LIST OF TABLES

1. SUMMARY

Using silk screened evaporated and sputtered Al as the metal source, we have studied the formation of Al back surface fields (BSF). The most satisfactory results were those obtained with the sputtered Al and in which open circuit voltages (V_{oc}) of 0.585v (12 Ω cm FZ silicon) have been achieved. The ultrasonic interconnect process is being verified. The process is generally satisfactory, but increased pull-strength may be obtained if some form of sintering is carried out on the metallized contacts. Plasma etching has been shown to be feasible as a replacement for wet chemical cleaning prior to diffusion. An IPEG calculation shows its cost to be $0.005/watt peak (1975$). Initial results on cells prepared by using electroless Pd/Ni plus either electroplated Ag or Cu have shown slightly poor performance than cells with the baseline evaporated Ti/Pd/Ag system. This is being further studied. A new mask has been designed for the 1.6 x 7.0 cm and 2.0 x 7.0 cm cells. This mask has a lower area coverage and total lower resistive loss than our previous mask design. It is also shown that the cell width should not exceed 2.0 - 3.0 cm for optimum efficiency.

2. INTRODUCTION

The major objective of this program is to define and verify a process sequence for the fabrication of solar cell modules from dendritic web silicon. Yet another objective is the development of key process steps. For such development, the process sequence must be amenable to automation and low cost manufacturing methods so that the target selling price of $0.50/watt peak (1975 $ in 1986) can be met.

Back surface fields (produced by a high/low junction at the back of the cell) are used to decouple the high recombination velocity ohmic back from the bulk of the material. This effect increases both V_{oc} and I_{sc} of the cell. For p-base cells, boron or aluminum is generally used to form the p^+ junction on the back of the cell. Previous work has shown that the type of p^+ region obtained by an aluminum alloying procedure is generally superior to boron diffused p^+ regions. At present, we have concentrated on several techniques for applying the aluminum to the back of the cell and on methods for alloying to form the p^+ region. Thus far, sputtered Al alloyed in either an rf furnace or resistance furnace gives the most uniform and reproducible results.

The plasma etching process uses gas compositions which can be broken down into a variety of active species by an rf glow discharge. These reactive components then combine with surface contaminants on the silicon surface to form volatile products which can be pumped out of the system. Plasma etching has been shown to be useful not only for this surface cleaning but also for removing photoresist, and in some cases etching the silicon surface. In this period, we have carried out a study which indicated that plasma etching could be used in place of the normal pre-diffusion cleaning of the dendritic web silicon. It has also been shown that this process is cost-effective, since the price is less than $0.005/watt in 1986 (1975 $).

The present metallization system used in this program is evaporated Ti/Pd + electroplated Ag. Although a very reliable system, its cost-effectiveness can be questioned because of the large capital expenditure required for vacuum systems. We are, therefore, investigating the applicability to dendritic web of an all-plated system (electroless Pd/Ni) as first described by Motorola. After the initial electroless plating, a thick conductive layer can be applied either by solder-dipping or electroplating Ag on Cu. The first experiments have shown that some changes are required in the Motorola process to fit our process sequence. Specifically, several of the HF etches must be deleted or modified due to their attack on the antireflection coating used in our sequence. Further tests are underway to determine the effectiveness and reliability of this system and a cost study comparing it to the evaporated plus plated technique will be made.

Parametric tests of the ultrasonic bonding are required to define acceptable operating regions. The parameters to be considered are bonding pressure, time and input power as a function of metallic contact and interconnect foil. The acceptable variation of these parameters within the operating region can be used to determine the amount of control required when an automated process is developed. These tests have been completed for copper and nickel ribbon to electroplated Ag.

The overall efficiency of a solar cell is influenced by the area coverage of the grid network used to collect the current. Nominal coverages using printed grids are 10-12% of the total area. This area is then unavailable for conversion of solar energy into electricity. Photolithographic techniques permit the use of thinner grid lines with a factor of two less area coverage. In this period a new mask design has been developed which considers and minimizes the resistive and area losses. This mask design, in conjunction with photolithographic techniques, should give efficient current collection at a coverage of about 3-5% of the total area of the cell. This technique should increase the absolute efficiency of the cell by 0.5 to 1%.

3. TECHNICAL DISCUSSION

3.1 Aluminum Back Surface Field Studies

3.1.1 Introduction

A high-low junction at the back of an n^+p solar cell (forming an n^+pp^+ structure) results in enhanced open circuit voltage and short circuit current. The V_{oc} is increased due to the reduced back surface recombination and the built in voltage of the p^+p region. Since I_{sc} is a function of V_{oc} it will also increase when a back surface field is present.

In the last quarterly report, we discussed how the back surface field operation and efficiency can be expressed using parameters relating to the p^+ and p regions. It was also shown that due to several factors (such as lower C_o and regrown layer thickness) Al BSF's may be preferable to those produced by a boron diffusion.

During this past quarter our experiments have concentrated on (1) methods for applying Al to the back surface of the cell and (2) methods of heating the cell and the temperatures required to drive in the Al.

The application methods were:

1. Silk screened Al paste (Englehard 3484).
2. Evaporated Al.
3. Sputtered Al.

The heating techniques were:

1. Resistance heated furnace (N_2 ambient).
2. RF heated furnace (H_2 or N_2 ambient).

Solar cell parameters and spreading resistance techniques are being used to determine the effectiveness of the several methods.

Insofar as the evaporated samples were concerned, we were unable to achieve uniform drive in depths,or reproducible alloying results. Although several possible reasons could be given for these results (e.g. back surface not sufficiently clean before evaporation), we will not pursue this technique any further.

3.1.2 Silk Screened Aluminum Paste

The samples were silk-screened using a prepared Al paste sold by Englehard Co. (#3484)*. The paste was applied using a 25 μm screen and the samples were dried at 200 - 250°C before any alloying procedure was attempted. After drying, the thickness of the paste was 20 - 25 μm and the density was estimated to be about 65% of the theoretical value.

To determine the effect of heating time and temperature on the thickness of the regrown layer and to determine an optimum time/temperature regime for alloying, samples of float zone p-type crystals screened with the Englehard paste were heated at 800°C, 825°C, and 850°C for 30 sec, 60 sec, and 120 sec. In nearly all cells, the screened material appeared to wet the surface uniformly and did not bubble up or lift off the surface. At higher temperatures and longer times,the crystals were warped and the 850°C/120 sec. sample fractured. This warpage was not apparently related to the degree of penetration and when the excess Al was etched off the back surface the crystal returned to its original flat form.

The depth of the regrown layer was measured by a spreading resistance technique on an angle lapped surface.

*Essentially similar results were obtained using an Alcoa paste.

An anomaly was noted in this series of tests. In two cases the dopant concentration profile indicated evidence of nonuniform alloying. This effect is shown in Fig. 1. In this figure, the depth into the crystal (in μm) vs. the dopant concentration is shown. As seen, there is an abrupt change in concentration at 2.8 μm with the regrown layer penetrating to 6.5 μm where the base dopant concentration is noted. This effect can be compared to a normal dopant concentration trace shown in Fig. 2. The sample showing the anomaly was etched and the area where the spreading resistance was measured was examined microscopically. A thin imperfection line was noted at the resistance discontinuity point. The chemical/crystallographic makeup of this band has not been determined. However, due to the nature of the spreading resistance technique, it probably represents a plane, perpendicular to the surface of the cell, where the paste did not alloy in.

There is another possible explanation for this data. The surface concentration on a number of these samples was near 10^{19} cm^3. This is too high for pure Al for which C_o should be 4-6 x $10^{18}/cm^3$. Therefore, it is possible that the noted profile is really the sum of the profiles of two impurities, one with a C_o of $10^{19}/cm^3$, the other (Al) with C_o of 5 x $10^{18}/cm^3$. We have contacted the supplier of the paste (Englehard Industries) and they state that in their analysis* In, B, or Ga (the most probable impurities) in the paste were not detected. At this point there is no firm conclusion as to the cause of the noted discontinuity.

The depth of the regrown layer determined from these measurements as a function of time and temperature is shown in Table 1. These data do not show the expected relationship between the thickness of the regrown layer and the time/temperature conditions, probably due to lack of control of important variables.

*Analyses made using emission spectroscopy.

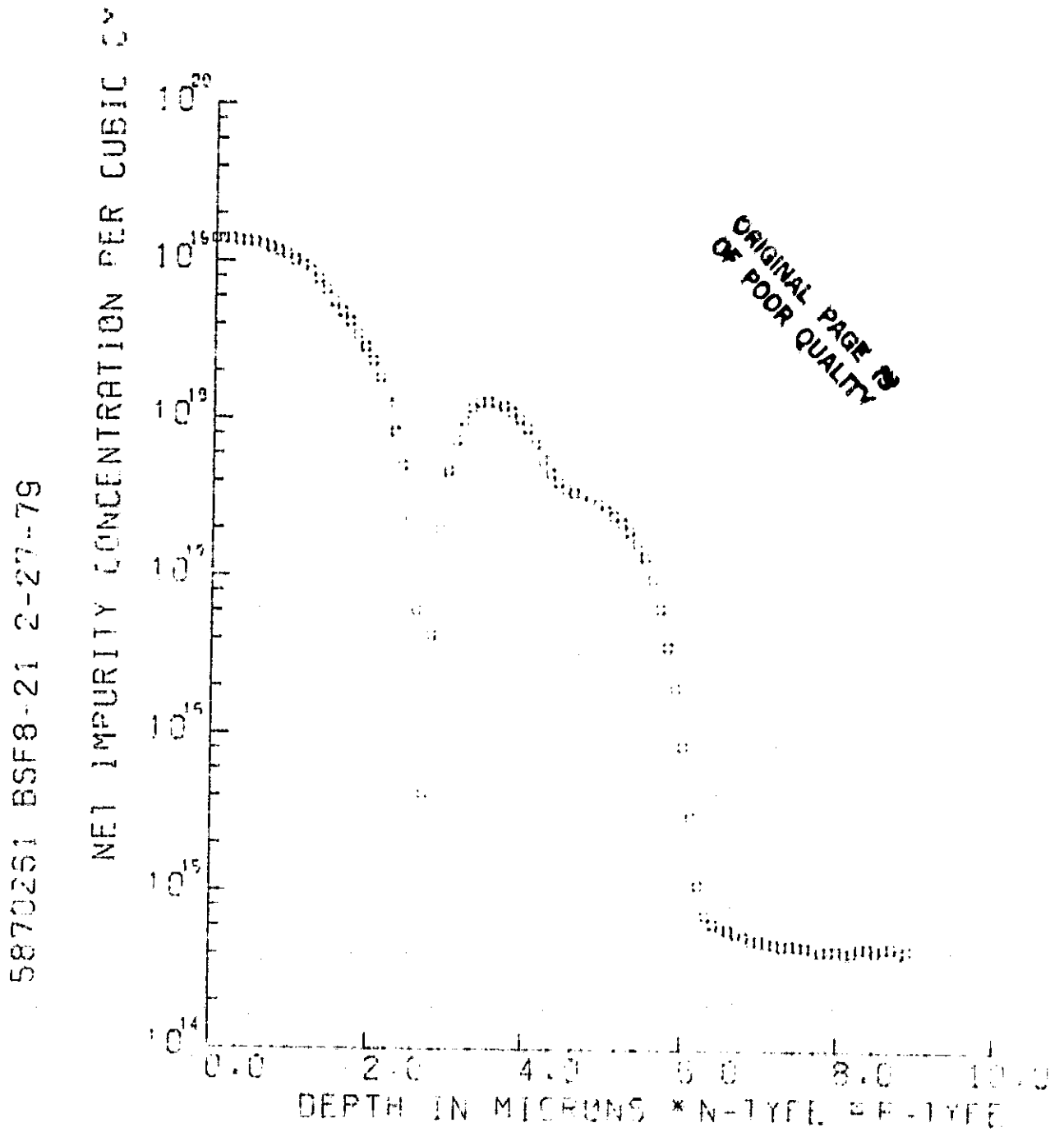

Fig. 1 Screened Al, alloyed at 800°C for 60 sec.

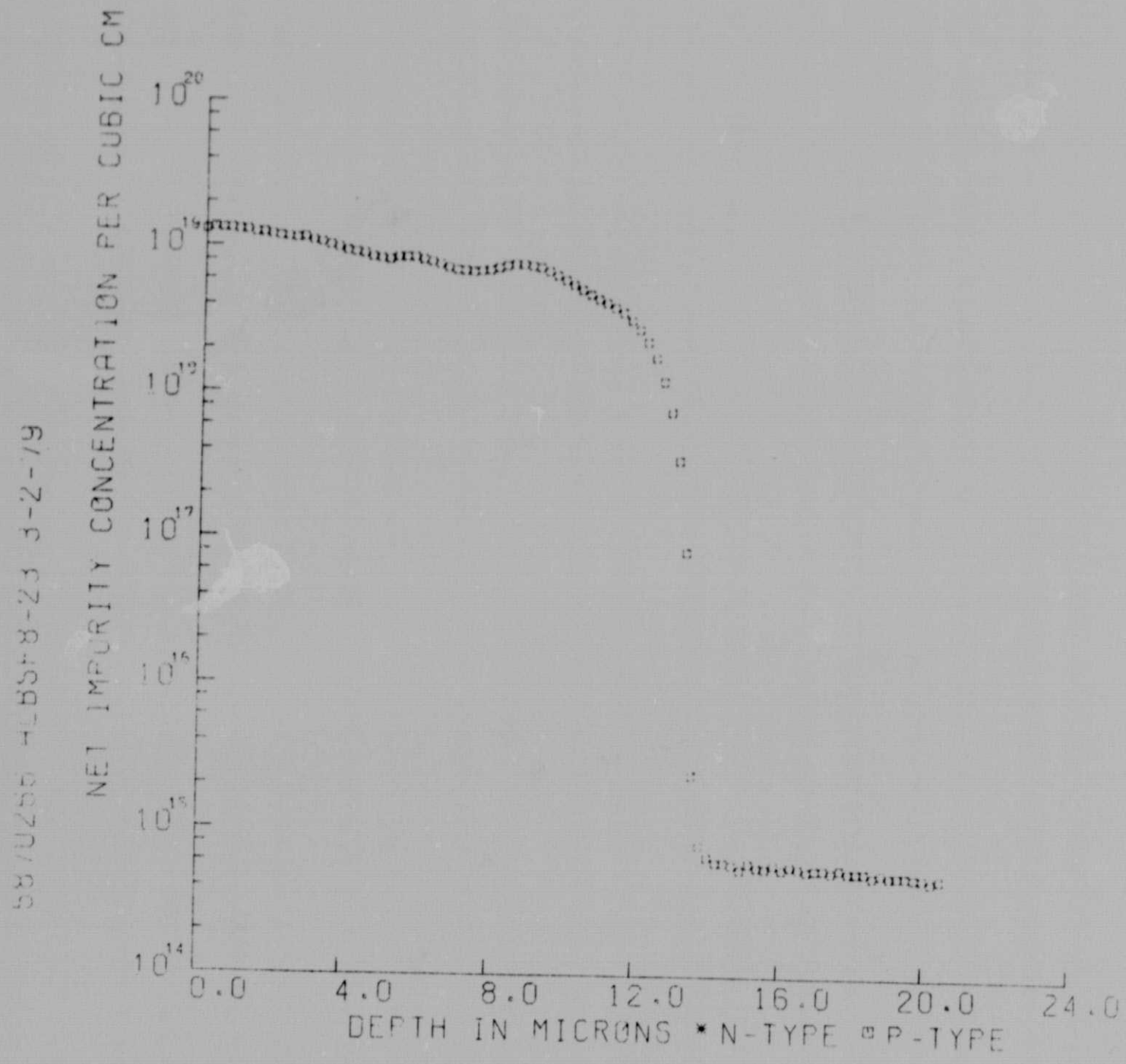

Fig. 2 Screened Al, alloyed at 825°C for 60 sec.

TABLE 1

Thickness of Regrown Layer at Various Times and Temperatures - Silk Screened Englehard #3484

Temp. (°C)	Time (Sec.)	Thickness of Regrown Layer (μm)
800	30	2.1
800	60	6.5
800	120	7.5
825	30	2.5
825	60	13.8
825	120	6.0
850	30	8.0
850	60	3.8
850	120	1.0

It may be noted that somewhat similar data was reported by W. Taylor et al. (Quarterly Report, October 1978, Spectrolab, Contract No. 954853).

These investigations show V_{oc} and I_{sc} peaking at certain firing times with both V_{oc} and I_{sc} lower at shorter and longer firing times. Our experiments were carried out in a resistance heated furnace in a nitrogen ambient, and it is quite probable that oxygen back-streamed into the furnace. Since the oxidation of the Al powder would occur more rapidly at higher temperatures, the Al on 850°C sample would oxidize more rapidly than that of the lower temperature samples. Therefore, in certain instances (e.g. high temperature) oxidation could impede the alloying process and reduce the regrown layer thickness.

This oxidation process does not completely explain the data in Table 1, but does give some idea of the complexity of the problem. Solar cells were fabricated on samples which had been silk-screened with the Englehard paste and alloyed at 850°C for 6 minutes and 8 minutes.

Table 2 shows representative data from these experiments. In most cases, the data are averages of 2 to 5 equivalently treated samples. In all cases, the front junction was phosphorous diffused with a junction depth near 0.4 μm.

In addition to the lighted I-V data given in the table, the I-V characteristics of selected samples were measured in the dark. In all cases, the shunt resistance exceeded 10^3 Ω and in most samples it exceeded 10^4 Ω. The average series resistance of 1-2 Ω was higher than the normal: 0.5 - 0.7 Ω. A 2 Ω series resistance is 2-4 times higher than desired and will depress the fill factor and correspondingly reduce the efficiency.

TABLE 2

Al Paste Alloyed BSF
(Phosphorous Diffused Front Junction; AM-1 — AR Coated)

Sample #	Alloy Cond. & Sample Ident	Penetration (μm)	V_{oc}(v)	I_{sc}(mA)	FF	Eff.(%)	τ_{OCD} (μsec)
15/16	6 min. at 850°C FZ crystal Al paste painted	< 1	.560	30.8	.61	11.2	9
18-11	6 min. at 850°C FZ crystal Silk screened paste	5.1	.585	31.6	.70	13.7	33
18-21 to 18-24	6 min. at 850°C FZ crystal Silk screened paste	5.0	.580	31.5	.64	12.3	30
20-1 to 20-4	8 min. at 850°C FZ crystal Silk screened paste	-	.550	30.5	.60	10.5	15

The samples painted with the Al paste showed essentially no penetration and a correspondingly low V_{oc}. This method of applying the Al was tested since silk-screening between the dendrites would have been difficult.

The float zone wafers with Al BSF having V_{oc} of 0.580 - 0.585 with effective lifetimes of 30-35 μsec show operational back surface fields. These values approach those achieved with evaporated or sputtered Al, but the low value of the fill factor reduces the cell efficiency.

These experiments are being repeated with Ampal #631 powder which is the preferred Al in process sequence given by Spectrolab.

3.1.3 Sputtered Aluminum Layer

Partly due to the nonuniformity and to the lack of reproducibility noted in the tests with evaporated and silk-screened aluminum, a number of experiments were carried out using sputtered Al on the back surface. In these trials, the phosphorous diffused web or float zone silicon was back-sputtered for 10 minutes (to clean the surface) before 10 μm of aluminum was sputtered.

The cells were heated in an rf furnace at 800°C, 825°C, 850°C, and 875°C in an H_2 ambient. In this process, the rf generator is preset to a power level so that the sample reaches the required temperature in about 30 sec. When the temperature is reached (as read by an IR pyrometer) the power is turned off and the sample cooled. With the inevitable slight overshoot in temperature, the sample is probably at the required temperature for 10-20 sec.

In general, these sputtered layers behaved well under the drive-in conditions. Over 90% of the samples showed a complete and uniform Al layer on the surface after the drive in. The remaining 10% showed areas where Al did not wet the Si.

Table 3 shows the results of these tests. The thickness of the regrown p^+ layer increased gradually with increasing temperature. The cell lifetime decreased slightly at the highest temperature and limited the V_{oc} enhancement and the efficiency. The maximum V_{oc} occurred at 850°C with .588V for the FZ material and with 0.577V for the web.

The p^+ layer is sufficiently thick that higher values of V_{oc} and efficiency would be expected. It appears that some lifetime killing mechanism is operating to reduce the maximum efficiency.

TABLE 3

CELL PARAMETERS - SPUTTERED AL

(12 Ω-cm Si)

Drive Temp. (°C)	p^+ thickness (μm)	Matl.	V_{oc} (V)	Eff. (%)	τ_{OCD} (μsec)
800	2	WEB	.577	14.5	20
825	6-8	FZ	.585	14.4	37
	3	WEB	.569	14.1	22
850	8	FZ	.588	15.2	34
	9	WEB	.577	14.8	26
875	9	FZ	.574	14.1	32
	5-10	WEB	.568	13.9	22

- AM-1; 100 mw/cm^2 -- AR coated
- Values given are averages of 8-10 cells
- Fired in rf heated furnace - H_2

3.1.4 Summary of Al BSF Studies

Table 4 summarizes the most important results reported in this quarter.

We have shown that surface cleanliness is important if uniform Al penetration is to be obtained. An H_2 ambient during firing will leave the residual Al suitable for contacting. Firing in O_2 will badly oxidize the Al and thus require secondary metallization. In the silk screened material, firing in a partial ambient of O_2 would remove more of the volatile organics.

The purity of the Al also effects the lifetime of the cell. The table indicates variation of a factor of 2.5 in lifetime for the various Al sources.

TABLE 4

IMPORTANT PARAMETERS - Al BSF FORMATION

- Silicon surface

  cleanliness important for uniform penetration

- Firing ambient

  H_2 preserves Al for contact, O_2 will completely volatize organics

- Al source

  purity will affect lifetime

Al Source	τ_{OCD} (μsec)
Sputtered	37
Evaporated	40
Silk screened	16

The lifetime data was obtained on floatzone silicon with equal thicknesses of the p^+ layer. It should be noted that the lifetime can be a function of base region degradation as well as performance of the back surface field.

3.1.5 BSF Processes — Costs

A preliminary cost estimate of the BSF processes was made earlier. These results, which include the cost of a $POCl_3$ diffusion, are shown in Table 5.

The cost difference in these three back surface processes is minimal. Thus, any decision regarding the type of BSF to be used can be made on technical grounds as opposed to cost factors.

TABLE 5

Value Added Costs* — BSF Processes

	BSF Process		
	B-diffused	Al Evap. + Drive	Silk Screened Al Paste + Drive
Value Added Cost (1975 $/peak watt)	0.048	0.040	0.035

3.2 Plasma Etching

The plasma etching process uses gas compositions, generally CF_4 and O_2, which are broken down into a variety of active species by rf glow discharge. These species form a low temperature, highly reactive plasma,and create volatile reaction products with surface contaminants on the wafer. The volatile products are then pumped out of the system.

This process was investigated as a substitute for the chemical cleaning of the dendritic web prior to diffusion. The grown web, at the present time, comes from the furnace coated with a lightly adhering brownish oxide.** In our standard processing, a wet chemical cleaning is used to remove the oxide layer and any impurities on the surface.

---

* Costs include $POCl_3$ diffusion + BSF process.

** It is anticipated that with further development, this oxide layer will not occur. However, at this time a chemical cleaning is required.

In the experiments reported here, some of the web samples were plasma cleaned/or etched with no prior cleaning while other samples were wiped with a $HF:H_2O$ solution. We have found that the latter is not a sufficient pre-diffusion cleaner method and must be followed by chelating with $H_2O_2:NH_4OH$ and $H_2O_2:HCl$.

Table 6 represents the results of these experiments. All tests were made on a single web crystal (RE 26-5) so that valid intercomparisons could be made. The plasma cleaning/etching was done in an LFE-301A reactor.

In Treatment 1, the as grown web with the oxide coating was plasma cleaned for 3 min. at 200 watts rf power with 300 cc/min. of O_2. Treatment #2 was the same as #1 except that PDE-100 (a proprietary etching gas produced by LFE Corporation) was substituted for the oxygen.

Treatments 3 and 4 were the same as 1 and 2 except that the web was lightly swabbed with an $HF:H_2O$ solution to remove the loose oxide film. Treatment #5 is our baseline cleaning process involving:

- HF/H_2O swab,
- Hot H_2SO_4 soak (2 min.),
- $NH_4OH:H_2O_2:H_2O$ chelating cleaning,
- $HCl:H_2O_2:H_2O$ chelating cleaning,
- DI H_2O rinse.

The data in Table 6 shows that Treatments 1 and 2 result in cells that are much poorer than the baseline treatment (#5). The major difference is in the V_{oc}, FF and lifetime. This would indicate that some lifetime killing impurities remained on the surface after the plasma treatment and diffused to the junction during the high temperature processing.

Treatments #3 and #4 result in cells that are as good as the baseline cells. It should be noted that when webs, which have only the HF cleaning procedure, are diffused, the results are always inferior to the baseline cleaning process since these indicate a 2% decrease in the efficiency. Therefore, it can be concluded that the plasma etching

TABLE 6

PLASMA CLEAN/ETCH TEST*

	Treatment	J_{sc} (ma/cm^2)	V_{oc} (V)	FF	Eff(%)	τ_{OCD} (μsec)
1.	Web - as grown + 3 min. plasma clean	32.3	.502	.689	11.2	6.2
2.	Web - as grown + 3 min. plasma etch	34.0	.514	.706	12.1	7.3
3.	Web - HF clean + 3 min. plasma clean	33.3	.545	.743	13.3	23.0
4.	Web - HF clean + 3 min. plasma etch	33.3	.541	.723	12.9	20.0
5.	Standard web cleaning process	33.2	.545	.737	13.1	24.7

*Web - RE 26-5: 10 Ω-cm; Boron BSF

AR coated

AM-1 - 100 MW/cm^2

or cleaning of HF cleaned webs is a suitable substitute for a baseline wet chemical cleaning.

In making a cost estimate of this process (IPEG methodology), we considered an output of 25 MW/yr. Other inputs in this calculation were one person (on site per shift) to handle the etching and the loading and unloading of cassettes. The electricity and cooling water usage was estimated from the power requirements of presently existing plasma etch apparatus.

The capital equipment cost of a plasma etch apparatus was estimated to be $500K. This equipment is designed to have sufficient throughput for the 25 MW output, and a cycle time of 5 minutes per batch was assumed. The other capital expenditure of $20K was for cassettes, holders, etc.

The etch and purge gas usage was calculated from equipments currently in use.

Using these inputs a value added cost of $0.05/Watt (in 1986, 1975 $) is obtained for this process. These data are given in Table 7.

3.3 Metallization

3.3.1 Metallization System

An additional vacuum deposition system has been set up to increase the throughput of metallized silicon. The system has a 4-packet electron beam gun with a 16 inch source to substrate spacing. Film thicknesses and rates are controlled with a quartz crystal monitor and Sloan rate controller. The thickness control and uniformity is expected to be within $\pm$ 10% over the deposition area. Special fixturing has been designed and fabricated to hold five strips (10 inches long) of silicon web in such a manner that both sides can be metallized with Ti/Pd/Ag during a single pump-down.

Figure 3 shows a photograph of the fixture mounted on its support frame inside an 18-inch bell jar. Very high purity source materials (titanium, palladium and silver) have been obtained, which are

TABLE 7

PLASMA ETCH - COST STUDIES

- IPEG Method
- Output - 25 mw/yr
- 3 stations - load cassettes
  etch
  unload to diffusion
- Costs

  Labor - 1 PY

  Utilities - 10^5 KH/yr (0.2 KWH/operating minute)

  Capital - 500 K$ (estimated from scale up of existing plasma etch equipment)

  - 20K$ (engineering estimate of cassettes, etc.)

  Commodities - 60 tanks each of etch gas and purge gas

  Floor Space - 150 ft^2

Value Added Cost - $0.008/watt (1986$) — $0.005/Watt (1986 in 1975 $)

Cost valid for both pre-diffusion cleaning and photoresist stripping

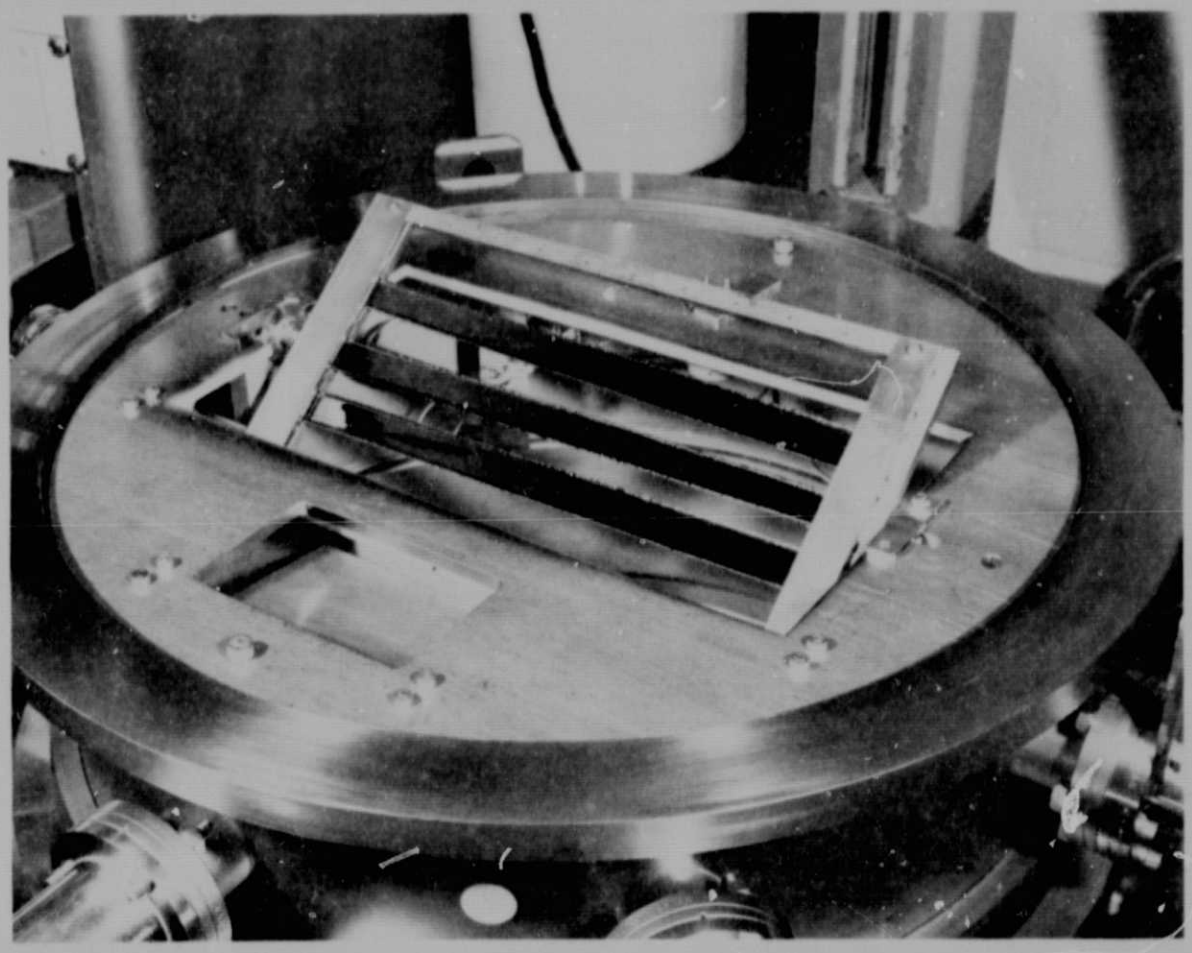

Figure 3. Fixture used to Coat both sides of Silicon Web with Ti/Pd/Ag during single pump-down

ORIGINAL PAGE IS
OF POOR QUALITY

vacuum melted and shaped to fit a Temescal STIH-270-2 electron beam gun copper hearth. It is anticipated that evaporated films made from these materials will contain a very low level of impurities. Typical lot analyses of these sources are shown in Table 8.

Such high purity material may not be required in a production process. However, impurities in contacting metals have been suggested as possibly causing cell degradation during contact sintering. Therefore, high purity metals are needed to determine if these impurities are a factor.

3.3.2 Contact Plating

Possible methods for lowering the cost of silicon solar cell processing are constantly being examined. To this end, we are investigating the electroless Pd-Ni plating system as described by Motorola. However, we are coating the Pd-Ni plated layers with electroplated Ag instead of dipping it into liquid solder.

In the Motorola process a dilute Pd solution is used to sensitize the silicon cell by a displacement reaction. This is followed by an electroless Pd solution utilizing an autocatalytic reaction for plating the Pd to the sensitized surface. After a heat treatment in nitrogen at 300°C, electroless Ni is plated onto the Pd surface. The final step in the Motorola process however, differs from that used by Westinghouse: in our method silver is electroplated over the Ni instead of solder over the Ni. The plating solutions used are given in Table 9.

A number of cells were fabricated, and the contact metallization, using the electroless Pd/Ni plus electroplated Ag system, was applied. In these tests, the antireflection coating (a TiO_2 and SiO_2 mixture) was used as a plating mask. Data on these cells are given in Table 10, cells 1 through 7. The column "Previous Data-Std. Processing" gives the results we obtained on the same web crystal using our standard evaporated TiPdAg system. These can be used to judge the effectiveness of the electroless PdNi system. In all cases where there are comparative data (cells 1, 2, 6 and 7), the cells with the electroless plating are inferior to the standard contacted cells. Data for the cells, after

TABLE 8

IMPURITY LEVELS IN ELECTRON-BEAM DEPOSITION SOURCE MATERIALS

Source Matl.	Impurity Levels (ppm)																										
	Al	Sb	As	Ba	Be	Be	B	Cd	Ca	Ce	Cu	In	Rh	Au	Os	Ir	Pd	Pt	Te	Mg	Hg	P	Pb	Nb	Ta	Ni	Fe	Co
Titanium (99.97%)	8																			10						5	80	
Palladium (99.99%)	3								3		5		15	4		10	Bal.	25								4	10	
Silver (99.999%)	<1										1			<1			<1			2							2	

Source Matl. (Contd.)	Impurity Levels (ppm)																				
	Mn	Zn	Ag	Na	K	Li	Ti	Sm	Mo	W	V	Gr	O	H	N	C	Ga	Ge	Si	Zr	Te
Titanium									3		15		420	64	48	10			12		Bal.
Palladium			5					5				3							10		
Silver			Bal.					<1											1.6		

(Source matls. supplied by Varian Specialty Metals Div.)

TABLE 9

PLATING SOLUTIONS

Palladium Sensitizing Solution

1. To 1500 ml of 50°C deionized water add 50 ml HCℓ and 0.04g of palladium chloride. STIR until solution.

2. Add 10 ml ammonium fluoride-stir.

Palladium Stock Solution

1. Add 10 ml of HCℓ and 1.9g of palladium chloride to 100 ml of 50°C deionized water - STIR.

Electroless Palladium Solution

1. Add 20 ml of palladium stock solution to 165 ml of NH_4OH. Allow to stand 1 hour and filter into 750 ml of deionized water.

2. Add 27g of $NH_4Cℓ$ and 3.75g sodium hypophosphate. STIR

3. Use solution at 50°C and a pH of 9.7-9.8.

Electroless Nickel Plating Solution

1. Dissolve 15g of nickel chloride in 440 ml of deionized water.

2. Add 25g NHCℓ, stir until dissolved. Add 42g sodium citrate, stir until dissolved. Add 5g sodium hypophosphate and 65 ml of NH_4OH. Stir until dissolved.

3. Use solution at 80°C and a pH of 10.0.

TABLE 10

Pd-Ni PLATING RESULTS
Plating Test 90322

		Previous Data-Std. Processing			As Plated			As Sintered 400°C/15 min		
		I_{sc}	V_{oc}	η	I_{sc}	V_{oc}	η	I_{sc}	V_{oc}	η
1.	RE24-1.4	27.9	.538	12.4	28.3	.498	10.1	28.0	.505	10.1
2.	RE24-1.4	27.9	.538	12.4	28.7	.508	11.2	28.4	.515	10.3
3.	W21-1.5				28.8	.510	11.1	23.6	.511	4.7
4.	W21-1.5				20.7	.448	3.2	22.0	.446	3.3
5.	W108-1.11				30.5	.514	9.9	29.7	.536	11.3
6.	RE9-3.4	31.0	.543	13.4	29.1	.524	11.7	28.0	.410	4.7
7.	RE9-3.4	31.0	.543	13.4	31.1	.461	7.2	29.8	.510	8.2
8.	RE1-1.4				30.1	.550	11.0	30.0	.557	11.3
9.	RE78-4.5	25.5	.525	10.7	29.6	.488	10.6	29.2	.495	11.2

AR Coated, AM-1

sintering at 400°C for 15 min., are shown in the third major column. These data are scattered and further tests are needed.

As stated above, cells 1-7 using the standard Motorola process were contacted, but the HF and aqua regia rinses were carried out for shorter lengths of time than suggested, since our antireflection coating was attacked by these chemicals. (The Motorola process uses silicon nitride as an antireflection coating which is generally impervious to these acids.)

After these tests, the Motorola process was modified so that the AR coating would not be disturbed. This modified process is shown in Table 11, and the parameters of cells contacted with this modified process are shown in Table 10, cells 8 and 9.

The data given in this section is preliminary. Although a large number of cells were used in the experiment, the yield of testable cells was small, and no definite conclusions can be drawn. A further experiment is in progress.

3.4 Ultrasonic Welding for Interconnection

The first series of bonding tests were made with the recently purchased Sonobond (Model W-1060D) welder shown in Fig. 4. Metal bonding parameters (force, time, and power) were selected based on previous experience with a similar unit at Sonobond Corporation and on trial runs on the new machine at Westinghouse. Copper, aluminum and nickel ribbons were bonded to plated silver and evaporated silver (Ti/Pd/Ag metallization). The bonds were pull tested and the interface after ribbon lift-off was examined and photographed at 100X. The results are summarized in Table 12. Aluminum tabs bonded to evaporated silver gave the highest average strength with the smallest standard deviation. Copper to evaporated silver and nickel to plated silver gave the highest bond strengths but poor reproducibility. An examination of the silicon surface (bond interface) after lift-off showed that the highest bond strengths correlated with significant cratering. The crater area was estimated, and the bond strength was calculated based on force per unit

TABLE 11

ELECTROLESS PLATING FOR Pd and Ni

1. Etch cells (NH_4+HCℓ+H_2O) to open grid in AR coating and rinse in DI H_2O (Use 60/40/100::NH_4F/HCℓ/H_2O)

2. Place cells into a teflon carrier and immerse into a palladium sensitizing solution under a high intensity light for 3 minutes while agitating gently. (Maintain high intensity light within 6 inches of the cells.

3. Rinse carrier and cells in running deionized water for 5 minutes.

4. Again immerse cells into the palladium sensitizing solution under a high intensity light for 5 minutes while agitating gently.

5. Rinse carrier and cells in running deionized water for 5 minutes.

6. Place carrier and cells into the electroless palladium solution (50°C) for 1 minute while agitating. Ambient light is kept low.

7. Rinse carrier and cells in running deionized water for 5 minutes. DRY

8. Place cells into a quartz boat and insert into a quartz tube furnace at 300°C write a N_2 flow for half hour. Cool.

9. Place cells back into carrier and immerse into a electroless nickel plating solution at 80°C for 5 minutes while agitating.

10. Remove carrier and cells from the nickel solution and rinse in running deionized water for 5 minutes.

11. Plate silver electrolytically.

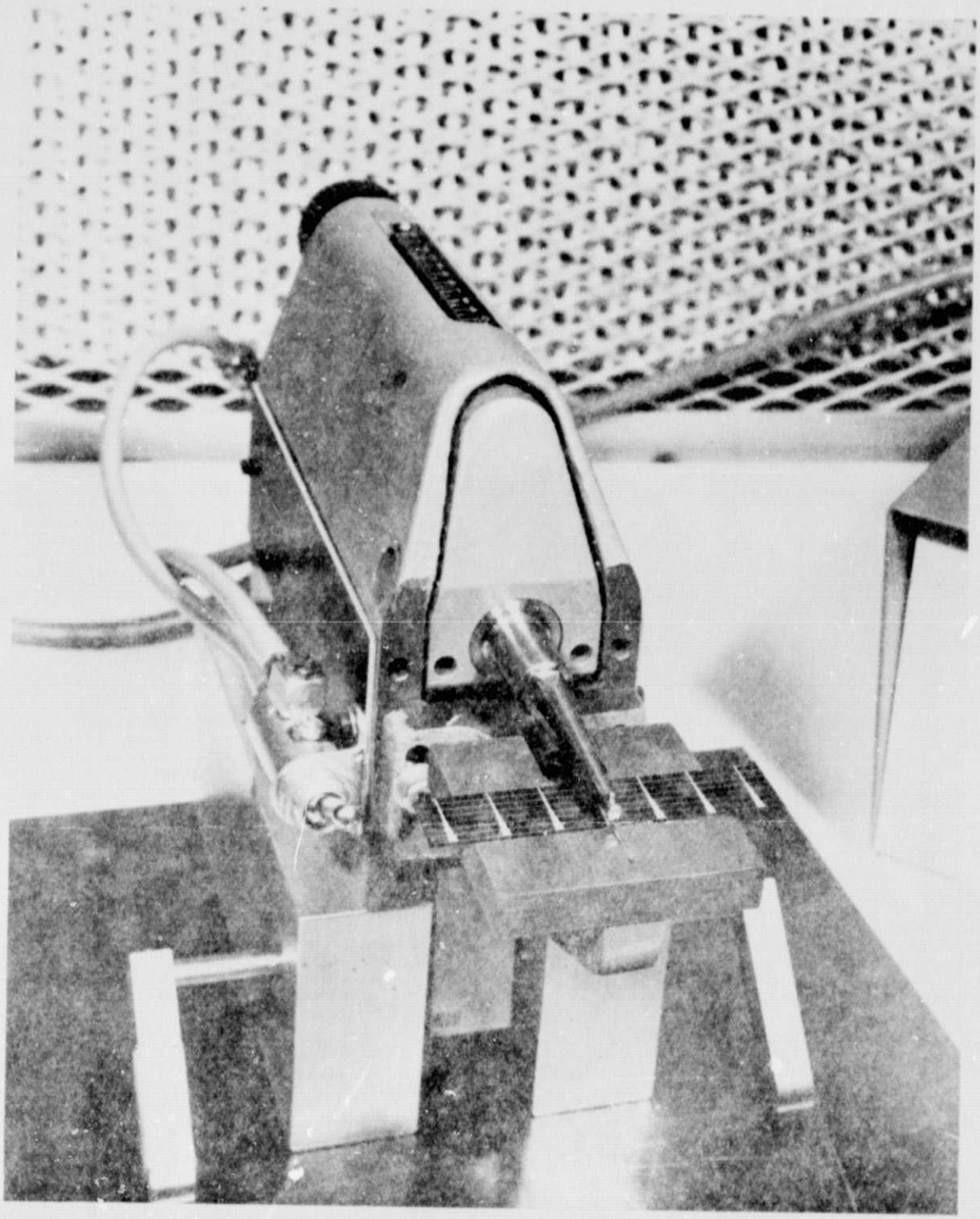

Figure 4. Sonobond Ultrasonic Weld Head (Model W-1060D)

ORIGINAL PAGE IS
OF POOR QUALITY

TABLE 12

RESULTS OF BOND TESTS
(SONOBOND W-10600 Welder)

Ribbon to Metal Surface	90° Peel Test			Bond Parameters			Interface Inspection
	Average (Grams)	Std. Dev.	MAX (MIN)	Power (Watts)	Force (OZ)	Time (Sec.)	
Copper (2 mil) - Plated Ag	32	57	118(0)	26	30	3	Cratering of Silicon (Concoidal fracture = High Str. Bonds)
Copper (2 mil) - Evap. Ag	109	73	181(14)	18	18		Cratering of Silicon (Concoidal Fracture = High Str. Bonds
Aluminum (1.5 mil) - Plated Ag	36	15	64(16)	18	18	.07	---
Aluminum (1.5 mil) - Evap. Ag	43	18	72(11)	17	21	.07	Cratering of Silicon (Matte Texture in Fracture Area)
Nickel (1.5 mil) - Plated Ag	94	133	188(0)	26	30	3	Cratering of Silicon (Concoidal fracture = High Str. Bonds)

area. Values ranging from 1000 to 3000 psi were typical. As is evident from these data, further tests are needed. The investigations revealed that the lack of reproducibility appeared to be the most significant problem which could have been the result of several factors:

- poor metallization adherence due to surface contamination
- movement or resonances in the silicon or metal tab during bonding (variations in energy coupling at the bond interface),
- room and table vibrations.

A second and more extensive group of bond tests, with copper and nickel ribbon ultrasonically welded to plated silver, have been completed. Bonds were made or attempted over a wide range of clamping forces, power, and weld time settings on the Sonobond unit. The objective of these tests was to determine the range of variables over which good bonds could be achieved and to identify those factors which contributed to bond strength variability in the first test series.

The 4 x 4 clamping force-power matrix in Fig. 5 shows the shaded area where bonds were observed for 1.5 mil thick copper ribbon to 4 μm thick electroplated Ag with an evaporated Ti/Pd underlayer. The weld time in this matrix was 1.2 seconds. The metallized cells used in these tests did not receive any post-deposition sintering since previous data showed that, on occasion, the sintering step resulted in some loss of cell efficiency. A similar 4 x 4 clamping force-power matrix was evaluated for shorter weld times (0.035, 0.10, and 0.2 seconds). No bonds were made at these time intervals for copper ribbon to plated silver, even at the highest force (38 oz) and power (30 watt) levels. A total of 48 trials were made (5 bond attempts at each power-force setting).

A similar series of tests were run for 2 mil thick high purity (> 99.99%) nickel ribbon to plated silver-metallized silicon web cells. Good bonds were observed in the shaded area of the 4 x 4 matrix (1.2 second weld times) shown in Fig. 6. Note that bonds were made at lower clamping forces (8 to 18 ozs.) compared to 24 to 38 oz. for copper ribbon (Fig. 5). The nickel ribbon welded at higher clamping forces adhered to the bonding tool tip rather than the cell.

Cu to PLATED Ag (T = 1.2 sec)

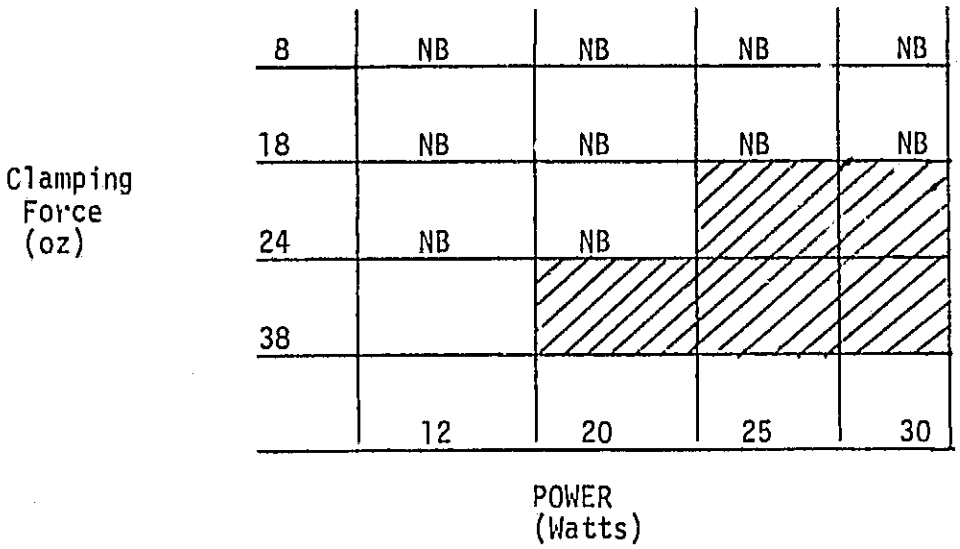

Shaded area - bonds made

NB - no bonding

Fig. 5. 4 x 4 clamping force - power matrix for copper ribbon ultrasonically welded to plated silver (1.2 second weld time)

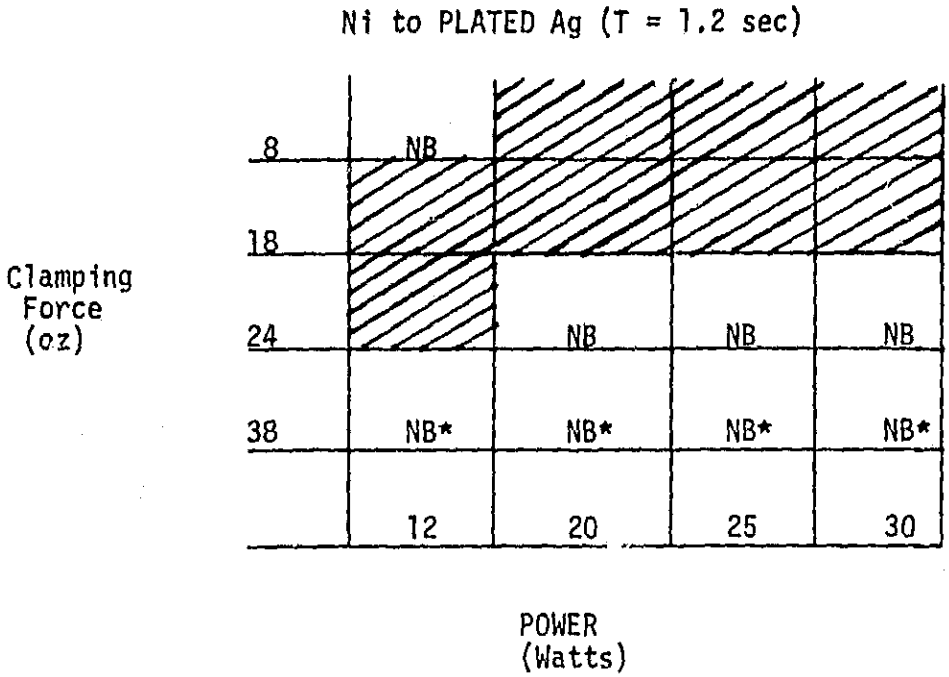

Shaded area - bonds made

NB - no bonding

NB* - Ni bonded to weld tip

Fig. 6. 4 x 4 clamping force - power matrix for nickel ribbon ultrasonically welded to plated silver (1.2 second weld time)

Table 13 shows the 90° pull-strength data for copper ribbon bonded to plated silver. The strength of 18 bonds was measured at the clamping force-power settings shown in the table. The overall average bond strength was 139 grams. An examination of the bond areas on the substrate and ribbon after the pull-test showed that most failures occurred in the copper ribbon rather than at the metallization-substrate interface. Typically, a small section of the ribbon was pulled-out and this section remained attached to the cell. The photomicrographs in Fig. 7 show the effect for two different copper to plated silver test specimens.

The bond strength data for nickel ribbon in Table 14 shows considerably more scatter than the results for copper ribbon, and the overall average strength is lower for 26 bonds (44 grams). Figure 8 shows a photomicrograph of the bond area on the cell for a high strength specimen (181 grams). A small piece of the nickel ribbon is still attached to the substrate. The bond area on the substrate for a lower strength specimen (22.7 grams) is shown in Fig. 9. The photomicrographs show that about one half of one bond area has a mirror-like surface (exposed silicon substrate) where the metallization was pulled away with the ribbon. The other half of the bond area containing a small section of the silicon cell pulled out, indicates that a metallurgical type bond was made in this area. These effects are typical for all of the bonds that were inspected at high magnification.

On the basis of these data and observations, it appears that the limiting failure mode is at the Ti/Pd/Ag-silicon substrate interface. High strength bonds would be more likely to be achieved with less variabilities and over a wider range of welding variables if the Ti/Pd/Ag adherence can be improved. This could be accomplished by post-deposition sintering or by sputter cleaning and/or sputter disposition of Ti/Pd/Ag. It is reasonable to assume that the energy introduced during ultrasonic bonding can result in appreciable localized heating in the bond area. The transient temperatures reached as a result of frictional heating especially at high power levels, high clamping forces, and long weld times are likely to exceed 500°C. A metallurgical bond is then made by a thermo-

TABLE 13

90° PEEL TEST DATA
1.5 MIL COPPER RIBBON BONDED TO PLATED SILVER (4μ)

Power (Watts)	Clamping Force (OZ)	90° Peel Strength Average (Grams)	Std. Dev.	Max.	Min.	Bonds Tested	Failure Mode
12	38	5	2	7.0	2.0	3	All metal ribbon - Metallization interface
20	38	189	28	209	169	2	Metal ribbon
25	38	19	--	--	--	1	--
	24	232	50	268	196	2	Metal Ribbon
30	38	149	117	331	0	8	Metal ribbon and Si Pull-outs
	24	216	11	223	209	2	Metal Ribbon
Average (All Bonds)		139	109	331	0	18	

Specimen #1 (100X)

Copper Ribbon

Substrate

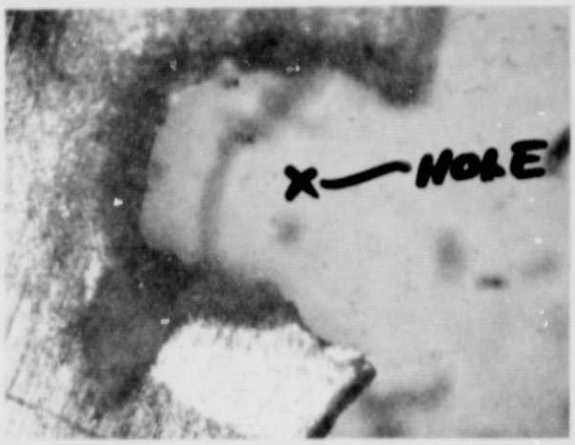

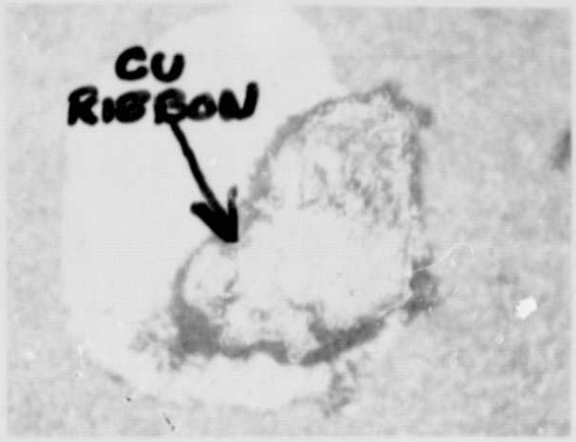

ORIGINAL PAGE IS
OF POOR QUALITY

Failed @ 69 grams

Failed at 69 grams
(note piece of ribbon
attached to substrate)

Specimen #2 (100X)

Hole pulled out of center of
copper ribbon
Failed at 223 grams

Fig. 7 Photomicrographs of failed bond areas for two different copper ribbon to plated silver test specimens

TABLE 14

90° PULL TEST DATA
2 MIL NICKEL RIBBON BONDED TO PLATED SILVER (4μ)

Power (Watts)	Clamping Force (OZ)	90° Peel Strength Average (Grams)	Std. Dev.	Max.	Min.	Bonds Tested	Failure
12	[illegible]	105	121	191	19	2	--
	18	4	2	5	2	2	--
20	18	47	37	100	9	6	Data scatter due to metallization failure (Fig. 9)
	8	25	35	50	0	2	--
25	18	96	69	181	23	5	Data scatter due to metallization failure (Fig. 9)
	8	18	16	32	0	3	--
30	18	15	13	26	0	3	--
	8	5	1	7	5	3	--
Average (All Bonds)		44	55	191	0	26	

Substrate Bond Area (100X)

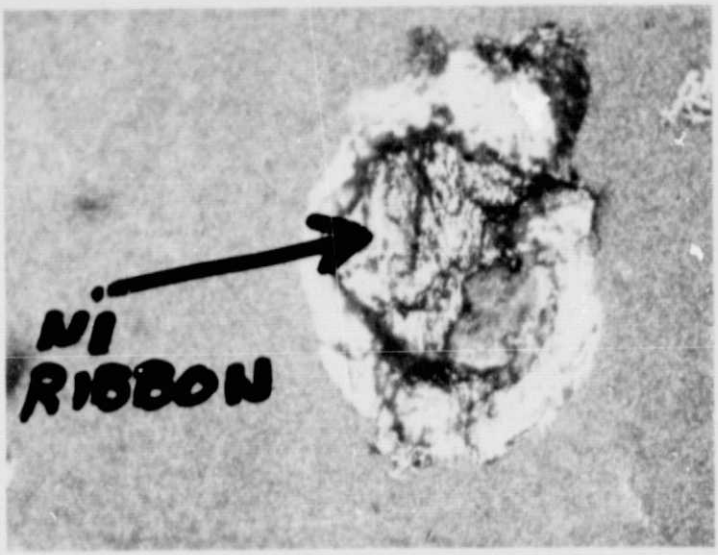

Failed at 181 Grams
(Note Piece of Ribbon Attached to Substrate)

Figure 8. Photomicrograph of the Bond Area on the Substrate for a High Strength Bond (Nickel Ribbon).

Substrate Bond Area (100X)

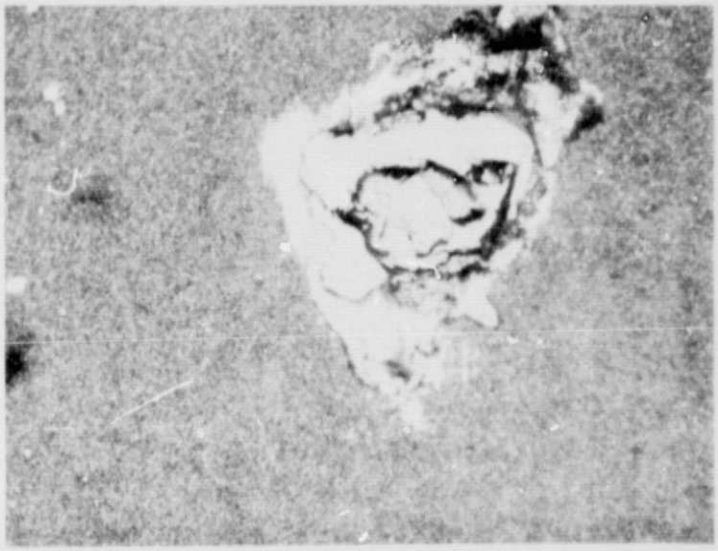

Failed at 23 Grams
(Note Mirror Surface and Crater Pull-Out)

Figure 9. Photomicrograph of the Bond Area on the Substrate for a Low Strength Bond (Nickel Ribbon).

compression mechanism. Copper ribbon bonds were strong only at high energy levels and no bonds were made at lower levels of energy. This would indicate that some form of metallization sintering took place during bonding. Nickel ribbon bonds were formed at low levels of energies but bond strengths were variable. This effect may be the result of localized differences in Ti/Pd/Ag adherence possibly induced during bonding.

3.5 Mask Design

One of the program objectives was to design a more efficient metallization grid pattern. That is, a grid pattern which collects the largest amount of current from the cell.

To derive the best grid configuration, the various loss mechanisms in the cell must be considered and their sum minimized. The grid pattern considered in these calculations is a series of straight lines emanating from a central pad at specific angles of a 1 cm long by "h" cm wide cell. The angles were chosen to give equal area sectors between the grid lines and the minimization discussed below was carried out only on this geometry.

The ohmic losses and the active area losses considered were:

1. sheet resistivity of the diffused surface layer,
2. resistivity of the grid fingers (assumed 10 μm high),
3. current loss due to active area of cell being covered by the grid finger, and
4. the interface resistance between the silicon and the metal contact.

To determine a minimum loss, the effect of these loss mechanisms were then integrated (by sectional integration) over the equal area sectors and minimized.

The first calculation determined the optimum number of grid fingers for a given finger width and for 1.6 cm and 2.5 cm wide cells. In this calculation, it is assumed that the grid pattern repeats every one cm; therefore, the results are valid for cells of any length.

Table 15 shows the results of this calculation for 25 μm and 50 μm finger widths. The term η/η_o is the ratio of the efficiency of the given grid configuration to a no loss configuration.

These indicate that for either the 1 mil or 2 mil finger width, four to five fingers are required per half cell.

It is instructive to determine the effect of the cell width on the normalized efficiency, η/η_o.* The calculation was carried for cells from 1 cm to 10 cm wide and for finger widths from 5 μm to 200 μm. This data is shown in Fig. 10. One factor to be noted is that there is a distinct penalty in efficiency incurred when wider cells are used, especially with narrow grid fingers. For the wider grid fingers (100 - 200 μm) this penalty is minimal up to a 4 cm wide cell. However, for the thinner grid fingers (25 - 50 μm), the difference between a 1 cm wide cell and a 4 cm wide cell is significant.

An implicit result of the data in Fig. 10 is that for higher efficiency cells, the grid finger width must be as small as possible, and no more than 50 μm wide. Such widths are attainable only by photolithographic techniques. The additional cost of this method (if any) must be considered in a trade-off with decreased cell efficiency when using wider grid fingers.

A new mask, incorporating the new pattern is now being prepared. 1.6 and 2.5 cm wide masks with grid fingers of 25 μm and 50 μm are being fabricated.

---

* η_o is defined as the efficiency of the cell when all ohmic and active area losses are zero.

TABLE 15

OPTIMUM NUMBER OF GRID FINGERS AT GIVEN
FINGER WIDTH FOR 1.6 cm AND 2.0 cm WIDE CELLS

Cell Width = 1.6 cm			Cell Width = 2.0 cm		
η/η_o	# Fingers	Width of Fingers (μm)	η/η_o	# Fingers	Width of Fingers (μm)
.970	4	25	.959	3	25
.970	5	25	.964	4	25
.969	6	25	.964	5	25
.958	4	50	.964	6	25
.965	5	50	.963	7	25
.948	6	50	.961	8	25
			.954	3	50
			.954	4	50
			.950	5	50
			.945	6	50
			.940	7	50

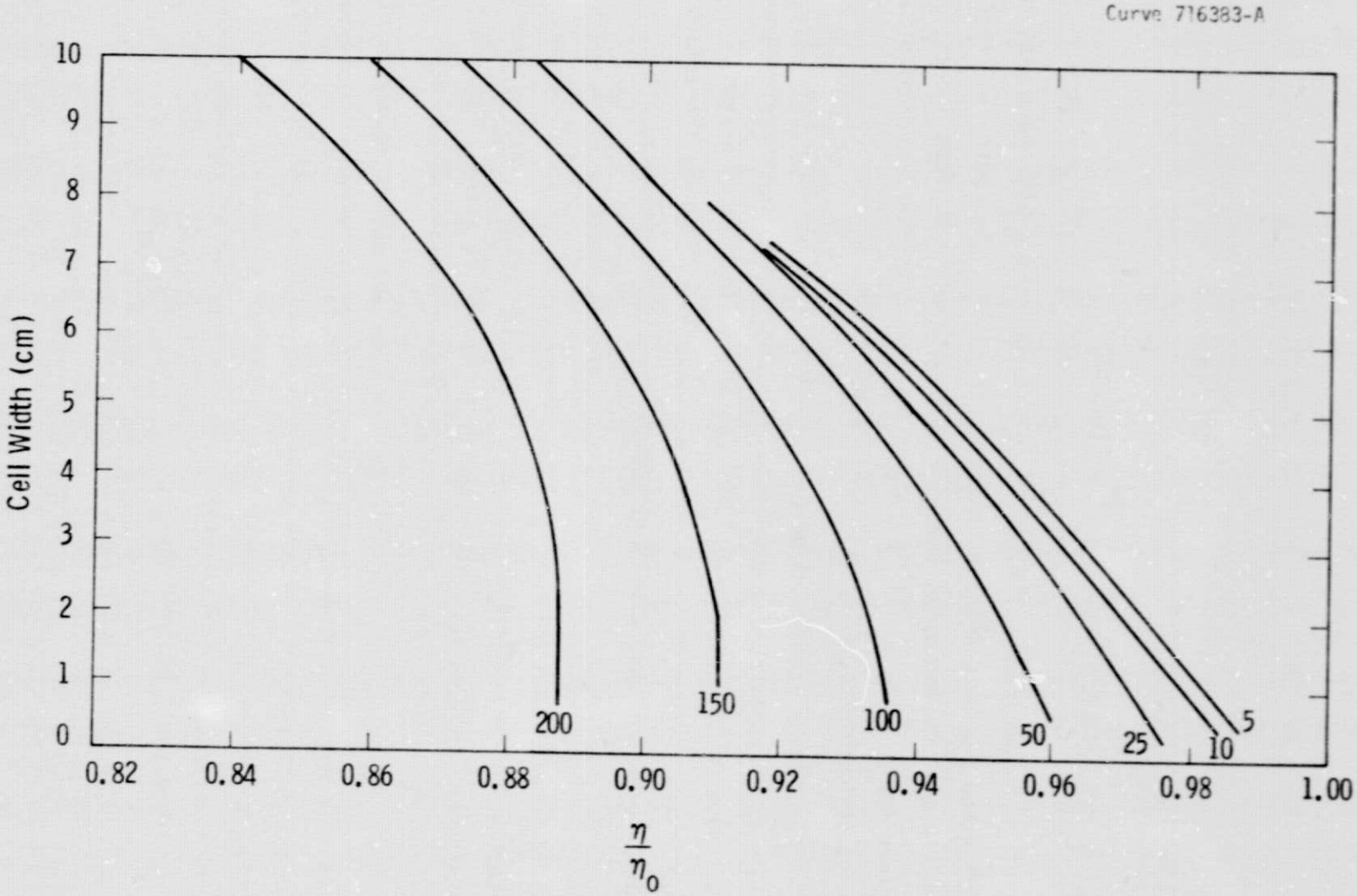

Fig. 10 Effect of cell width on efficiency at several grid finger widths.

4. CONCLUSIONS

Evaporation, silk-screening and sputtering have been used to apply Al to the back surface of the solar cells. The sputtered layers show the most reproducible behavior when alloyed in to form a back surface field. The sputtered layers wet the Si surface more uniformly during the alloying and give uniform penetration.

Plasma etching of dendritic web silicon has been shown to be a suitable substitute for pre-diffusion wet chemical cleaning. Results equal to base line processing were obtained using either oxygen or a proprietary etching gas. It was found necessary, however, to remove loosely adhering oxides with HF before the etching process.

It has been shown that the electroless plating of Pd and Ni can be incorporated into our process sequence. Minor modifications are required in the process specified by Motorola since our dip applied antireflection coating is attacked by the cleaning acids. The anti-reflection coating does act as a plating mask during the process.

Ultrasonic welding tests of copper and nickel ribbon to electroplated Ag show the major failure made is at the TiPdAg-Si interface. Average pull strengths of 139 gm and 44 gm were measured for copper and nickel respectively. Although these bonds are presumably adequate for manufacturing, the bond strength could be improved if the adherence of the TiPdAg could be improved.

5. PROGRAM STATUS

5.1 Present Status

We have completed the experimental work on plasma etching and a value added cost using the IPEG method has been obtained. A complete SAMICS cost will be obtained in the next period.

Thus far, alloyed in sputtered Al has given the most satisfactory back surface field structure data on silk screened samples using "AMPAL" Al powder was delayed until all materials were available.

Verification tests of the ultrasonic welding technique indicates that some contact sintering may be desirable.

5.2 Future Work

The entire SAMICS input for our process sequence is being reworked. The inputs are being verified and where required, changed. Once the baseline sequence is run, a number of iterations of back surface field costs, plasma etch costs, effect of web width, etc. will be studied.

Further tests will be made on the electroless Pd/Ni plus electroplated Cu system. These tests, together with a cost study, should indicate their cost effectiveness for the processing sequence.

During the next quarter, initial panel fabrication will start.

6. ACKNOWLEDGEMENTS

The authors wish to acknowledge the valuable assistance of the following: Dr. S. Farukhi for editing the manuscript and preparing it for publication; H. Abt, W. Cifone and J. McNally for cell fabrication; D. Schmidt for testing and data reduction.